HEALTH AND MEDICINE

Novel fractionated ultrashort thermal exposures with MRI-guided focused ultrasound for treating tumors with thermosensitive drugs

Marc A. Santos[1,2], Sheng-Kai Wu[1,2], Maximilian Regenold[3], Christine Allen[3], David E. Goertz[1,2], Kullervo Hynynen[1,2,4]*

Thermosensitive liposomes represent an important paradigm in oncology, where hyperthermia-mediated release coupled with thermal bioeffects enhance the effectiveness of chemotherapy. Their widespread clinical adoption hinges upon performing controlled targeted hyperthermia, and a leading candidate to achieve this is temperature-based magnetic resonance imaging (MRI)–guided focused ultrasound (MRgFUS). However, the current approach to hyperthermia involves exposures lasting tens of minutes to hours, which is not possible to achieve in many circumstances because of blood vessel cooling and respiratory motion. Here, we investigate a novel approach to overcome these limitations: to use fractionated ultrashort (~30 s) thermal exposures (~41° to 45°C) to release doxorubicin from a thermosensitive liposome. This is first demonstrated in a dorsal chamber tumor model using two-photon microscopy. Thermal exposures were then conducted with a rabbit tumor model using a custom MRgFUS system incorporating temperature feedback control. Drug release was confirmed, and longitudinal experiments demonstrated profoundly enhanced tumor growth inhibition and survival.

INTRODUCTION

Improving the delivery of chemotherapy to solid tumors while minimizing their harmful side effects is a central challenge in medical oncology. A promising alternative paradigm to conventional chemotherapeutic drug administration is to use thermosensitive liposomes (TSLs), which release their drug payload within the hyperthermia regime, i.e., 41° to 43°C (*1*). In addition to enabling localized triggered release, hyperthermia offers several additional benefits such as reduced tumor interstitial fluid pressure (*2*), increased vessel permeability (*3*), perfusion and oxygenation within the heated tumor (*4*), and stimulatory effects on the immune system (*5*). This creates an advantageous environment for drug delivery as the heat treatment allows more bioavailable drug to reach the tumor site while potentiating the cytotoxicity of drugs (*6*) without adding any additional toxicity for the patient (*7*). A wide range of thermosensitive carriers are under development (*8*); the most advanced of these in terms of clinical evaluation is the doxorubicin-loaded TSL (TSL-Dox) ThermoDox, which has undergone clinical trials for liver cancer in combination with radiofrequency ablation (*9*). Despite encouraging results in subsets of patients, it was hindered by a lack of effective temperature control.

The ability to perform fully noninvasive, targeted, and controlled hyperthermia exposures would greatly expand the utility of thermosensitive liposomal drugs, and a leading candidate for doing this is focused ultrasound (FUS) (*10*). Recently, the clinical feasibility of using FUS to generate mild temperature elevations for 30 to 60 min within liver tumors and the subsequent release of doxorubicin from ThermoDox was investigated (*11*). Temperature monitoring was performed at single locations in a subset of patients using a thermocouple, and respiratory motion was mitigated with jet ventilation and general anesthesia. Doxorubicin delivery was demonstrated, though with considerable variability, which was likely due to tumor temperature heterogeneity (*12*). This was an important first result, but it also highlights that more effective temperature control over tumor temperatures is required. Magnetic resonance imaging (MRI)–guided FUS (MRgFUS) can achieve noninvasive temperature-controlled heating of tissues (*13*). Previous preclinical MRgFUS studies demonstrated drug delivery (*14*) and significant antitumor effects (*15*) when temperatures were maintained at 42°C for 20 min with TSL-Dox. The aforementioned studies followed the established approach to hyperthermia, which is to maintain temperature elevations for tens of minutes to several hours. However, this is challenging to do in many clinical situations because of respiratory motion, heating of nearby bone, and convective blood vessel cooling.

In this study, we investigate a new framework for hyperthermia to treat tumors with TSLs, which is to fractionate heating into ultrashort (~30 s) thermal exposure sequences using MRgFUS. While conceptually simple, this is counter to the established dogma of using long-duration continuous hyperthermia exposures and has important implications for overcoming key limitations that impede the clinical viability of thermosensitive liposomal therapy. By reducing the duration of an individual thermal exposure fraction to 30 s, this enables it to be implemented within a patient breath hold, reducing motion effects on temperature measurements and targeting, as well as mitigating blood flow and bone heating effects. We first examine the release and uptake of doxorubicin from TSL-Dox with ultrashort hyperthermia sequences (10×, 30 s at 41° to 45°C) in a dorsal chamber murine tumor model using in vivo two-photon microscopy. We then develop the first implementation of fractionated ultrashort thermal exposures using a custom MRgFUS system and show in a rabbit tumor model that it produces targeted drug release from TSL-Dox that is associated with profoundly enhanced tumor growth inhibition and survival.

[1]Physical Sciences Platform, Sunnybrook Research Institute, Toronto, ON, Canada. [2]Department of Medical Biophysics, University of Toronto, Toronto, ON, Canada. [3]Leslie Dan Faculty of Pharmacy, University of Toronto, Toronto, ON, Canada. [4]Institute of Biomaterials and Biomedical Engineering, University of Toronto, Toronto, ON, Canada.
*Corresponding author. khynynen@sri.utoronto.ca

RESULTS

Ultrashort FUS thermal exposures release doxorubicin from TSL-Dox in mouse tumors

Doxorubicin release from a commercial formulation of TSL-Dox (ThermoDox, Celsion Corporation) was observed in real time using in vivo two-photon microscopy during ultrashort (~30 s) FUS thermal exposures (41° to 45°C). When in liposomal form, doxorubicin fluorescence is optically quenched and effectively undetectable, but when in "free" form, it is readily detectable, thus providing a means by which to visualize its release. The imaging paradigm used in these experiments is shown in (fig. S1A). A photograph of the experimental setup containing the two-photon compatible ring transducer and the FaDu xenograft tumor in a mouse dorsal skinfold window chamber is shown in (Fig. 1A). A representative two-photon image of the fluorescein isothiocyanate (FITC)–labeled microvasculature and the presence of FaDu tumor cells expressing green fluorescent protein (GFP) is shown in (Fig. 1B). Individual, controlled ultrashort thermal exposures to 41°, 42°, 43°, and 45°C were achieved with real-time thermocouple-derived temperature-based feedback using a proportional integral, and derivative (PID) control algorithm (Fig. 1C and table S1). Example two-photon images shown in (Fig. 1D) illustrate drug release within the vessels and uptake by the surrounding tumor cells before, during, and after heating to 43°C. After treatment, the doxorubicin fluorescence is well localized within the tumor cell nuclei outside of the FITC-labeled vasculature. A quantification of the intravascular signals as a function of time for the four temperatures is shown in (Fig. 1E). In all cases, the released drug signal in the intravascular compartment appears highest after the first exposure and then diminishes with each successive burst (6-min intervals), consistent with the plasma pharmacokinetics of TSL-Dox. In general, the mean values of the intravascular signal at a given time point are higher with increased temperatures, except for the 45°C case, which begins to fall below the 43°C case following the second heating point. A quantitative intergroup analysis of variance (ANOVA) of the area under the curve from 0 to 60 min for the different groups did not reach statistical significance ($P = 0.17$).

The extravascular compartment drug signals are shown as a function of both time and distance from vessel boundaries in (Fig. 1, F to I) and in terms of the mean extravascular signals in (Fig. 1J). The 41°C case shows a modest increase over baseline and fluctuates over time. For the 42° and 43°C cases, drug signals increase with the target temperature and with each successive exposure with the rate of increase slowing over time. In the case of 45°C, the extravascular doxorubicin signal appears to reach a peak at the 24-min time point (Fig. 1J), or after four exposures, and then plateaus. Figure 1K shows the mean extravascular signal at 60 min following the infusion of TSL-Dox when the exposures ceased. At this point, the 41°C exposure has resulted in a modest level of delivery, consistent with the nominal release threshold for TSL-Dox being in the ~41.3°C range. However, the drug signal level was significantly elevated at 42°C versus 41°C (74 ± 17% versus 21 ± 9% I_0, $^*P = 0.03$) and at 43°C, the drug signal approached significance compared to 41°C (67 ± 33% versus 21 ± 9% I_0, $P = 0.06$). Notably, the 45°C exposure level drug signals were not significantly higher than for the 41°C case (62 ± 41% versus 21 ± 9% I_0, $P = 0.09$), and they exhibited a considerable degree of variance between tumors. It was also observed, as shown in (fig. S1, B to E), that the 45°C exposures resulted in overt signs of acute vascular damage such as flow cessation and hemorrhage, generally after two to three exposures. The compromised microvasculature was presumably a factor that inhibited further extravasation of the circulating drug and gave rise to a variable degree of delivery by the end of treatment.

Collectively, these data demonstrate that ultrashort thermal exposures can release doxorubicin from TSL-Dox that is subsequently taken up by tumor cells and, on the time scales assessed, the level of doxorubicin signal in the extravascular space increases with the number of exposures, subject to the pharmacokinetics of TSL-Dox in the plasma. The ultrashort thermal exposures to 42°C appeared to result in the most consistent amounts of increased drug delivery in mouse tumors and were therefore chosen to be evaluated on their therapeutic efficacy in rabbit thigh Vx2 tumors using MRgFUS.

Fractionated ultrashort MRgFUS heating in rabbit Vx2 tumors

The therapeutic impact of the ultrashort sequences in combination with TSLs was assessed using tumors situated in rabbit thighs. This is an approach that has previously been used for long-duration heating and provides a more clinically relevant spatial scale for heating and control with MRgFUS (*14*). Along with MRgFUS heating in ultrashort fractions with TSL-Dox, both TSL-Dox and MRgFUS heating alone were evaluated on their antitumor efficacy. The short-duration heating using temperature feedback control was implemented on a custom MRI-compatible FUS system featuring a single-focus transducer that achieves tumor coverage by translating through a series of discrete locations. A diagram of the experimental setup is shown in (Fig. 2A), and an MR image depicting the setup is shown in (Fig. 2B). First, tumors were identified with gadolinium-enhanced MRI (Fig. 2, C and D) at which point discrete regions of interest (ROIs) were chosen to cover the tumor (Fig. 2E), and the order of treatment was selected to prevent the heating of immediately adjacent ROIs and unwanted overheating of the tumor to potentially ablative levels. Next, either TSL-Dox or a control, dextrose alone (Fig. 2F), was administered, and MR thermometry was used to provide real-time temperature feedback during the heat treatment (Fig. 2, G and H). To potentiate the release of doxorubicin from TSL-Dox, each ROI was heated discretely for 30 s up to 42°C for a total of 10 times.

The core temperature of the rabbits in the groups receiving MRgFUS alone or MRgFUS+TSL-Dox were 35.0 ± 0.3°C and 34.9 ± 0.7°C ($P = 0.62$), respectively, which is below the physiological level in rabbits and in humans. The real-time temperature control algorithm was able to achieve similar temperature responses in both groups receiving MRgFUS. The mean temperature within the tumor ROIs was used for feedback, and the mean temperature achieved in the MRgFUS alone (Fig. 3A) and the MRgFUS+TSL-Dox group (Fig. 3B) was 42.1° ± 0.3°C and 42.0° ± 0.4°C ($P = 0.60$), respectively. The distribution of tumor temperatures within the heated ROIs was compared by analyzing the temperatures that 10% (T_{10}) and 90% (T_{90}) of the voxels within the ROI exceeded. The T_{10} values were found to be 43.4° ± 0.4°C and 43.7° ± 0.6°C ($P = 0.30$) for the groups receiving MRgFUS alone or MRgFUS+TSL-Dox, respectively, and the T_{90} values were 40.7° ± 0.4°C and 40.1° ± 0.7°C ($P = 0.10$). Collectively, these data demonstrate that the ultrashort heating approach is feasible and can be achieved in a controlled and reproducible manner in rabbit thigh tumors.

An important metric in thermal therapy is "thermal dose," which is used to provide an indication of the bioeffects that can be expected to result from the therapy. This is frequently expressed in terms of cumulative equivalent minutes at 43°C (CEM_{43}) in recognition that

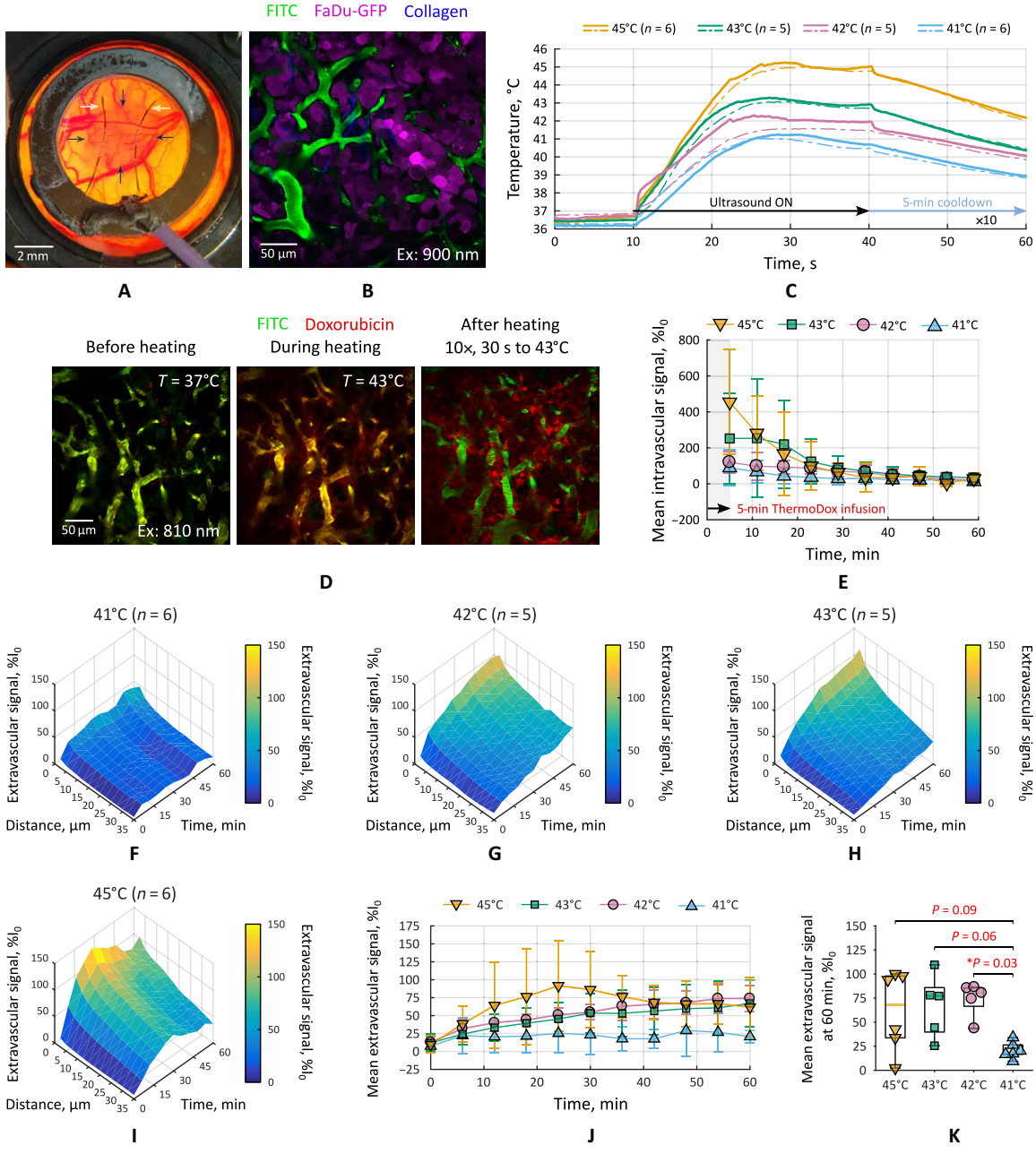

Fig. 1. Two-photon visualization of doxorubicin release and uptake in mouse tumors during ultrashort FUS thermal exposures. (**A**) Illustration of two-photon compatible ring transducer coupled to a FaDu-GFP tumor (black arrows) with implanted thermocouples (white arrows) for temperature feedback. (**B**) Representative image of the FITC-labeled microcirculation (green) within the FaDu-GFP tumor, whose cells are false-colored magenta under 900-nm excitation. (**C**) Example temperature profiles within the dorsal window chamber at different target temperatures using real-time feedback control. (**D**) Changes of the fluorescent signal, indicating the release of doxorubicin, under 810-nm excitation within the FaDu-GFP tumor after heating to hyperthermia temperatures in real time and after 10 ultrashort thermal exposures to 43°C. Tumor cells were not visible under 810-nm excitation. (**E**) Means ± SD of the intravascular drug signal measured during FUS hyperthermia at each temperature level. Surface plot of the mean doxorubicin fluorescent signal in the extravascular space as a function of distance to the nearest vessel and time, averaged for each mouse tumor heated to (**F**) 41°, (**G**) 42°, (**H**) 43°, and (**I**) 45°C. (**J**) Mean fluorescent signal in the extravascular space continues to increase after successive 30 s of heating, indicating that more and more drug is being delivered to the tumor at each hyperthermia temperature elevation. (**K**) Box-and-whisker plots indicating all data points at the 60-min time point comparing the mean doxorubicin signal in the extravascular compartment at each temperature exposure. The groups were compared using one-way ANOVA with Bonferroni post hoc tests for multiple comparisons; $^*P < 0.05$.

both the absolute temperatures and the duration of elevation are relevant to inducing thermal bioeffects. The spatial median thermal dose across the heated ROIs in Vx2 tumors was not significantly different between the MRgFUS alone and MRgFUS+TSL-Dox groups, with values of 2.8 ± 0.9 CEM_{43} and 3.2 ± 1.0 CEM_{43} ($P = 0.54$) being attained respectively. An example image depicting the spatial distribution of thermal dose is shown in (Fig. 3C). Greater variation was observed with thermal dose calculations from the T_{10} temperature

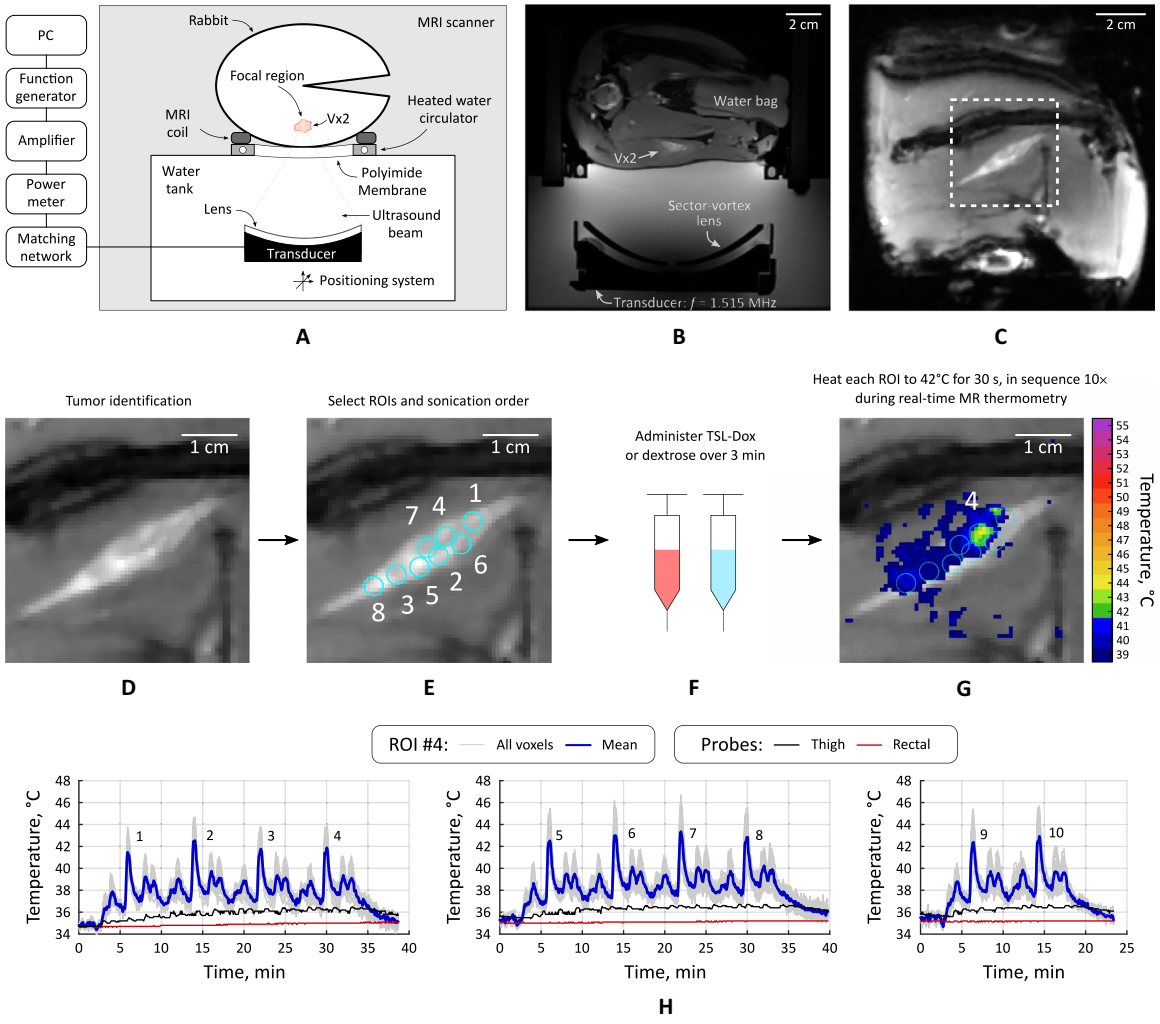

Fig. 2. MRgFUS treatment planning and tumor temperature profile. (**A**) Schematic diagram of the MRgFUS experimental setup. (**B**) Axial contrast-enhanced T1-weighted MR image of a tumor-bearing rabbit within the MRI-compatible FUS setup. (**C**) Coronal MR image within the plane of the Vx2 tumor for targeting and MR thermometry feedback purposes. Experimental paradigm, which involves (**D**) tumor identification, (**E**) followed by the selection of ROIs within the tumor that will be heated discretely, (**F**) the administration of TSL-Dox or dextrose alone depending on the treatment group, and (**G**) real-time MRgFUS heating of the target tumor. Rabbits receiving TSL-Dox alone did not have their tumors heated with MRgFUS. (**H**) Temperature profile within ROI #4 throughout the entire heat treatment, which consisted of heating all eight ROIs to 42°C for 30 s, 10 times in sequence.

profile in each ROI, which attained significantly different thermal dose values of 7.9 ± 2.0 CEM_{43} and 14.0 ± 5.5 CEM_{43} (*P = 0.04) in the MRgFUS alone and MRgFUS+TSL-Dox groups, respectively. The thermal dose calculated from the T_{90} temperature profile did not show a significant difference, with values of 0.4 ± 0.2 CEM_{43} and 0.4 ± 0.5 CEM_{43} (P = 0.92) being attained for the MRgFUS and MRgFUS+TSL-Dox groups, respectively. Tabulated values comparing the heating results across tumor-bearing animals are displayed in (Table 1).

The similarities in the baseline characteristics and the temperature elevations in the rabbits receiving MRgFUS and MRgFUS+TSL-Dox suggest that any therapeutic effect from the heat treatment itself would be similar in both groups.

Doxorubicin delivery in Vx2 tumors following fractionated ultrashort MRgFUS thermal exposures

At 4 hours after drug administration [doxorubicin (8.35 mg/kg), TSL-Dox] and MRgFUS short-duration heating in one of the bilateral Vx2 tumors, the tumors were excised and sectioned for histological analysis with confocal microscopy. The mean temperature profile within the heated tumor ROIs, tumor delineation, and thermal dose in the heated Vx2 are shown in (Fig. 3, D to F). Following the experimental paradigm in (Fig. 4A), example whole-tumor sections are shown in (Fig. 4B), and the autofluorescent doxorubicin signal is noticeably more pronounced in heated Vx2 tumor sections compared to unheated ones. At increased magnification, shown in (Fig. 4C), doxorubicin fluorescence is well localized within the 4′,6-diamidino-2-phenylindole (DAPI)–stained nuclei around the CD31-stained endothelial cells. The amount of fluorescence is markedly increased in the heated compared to unheated Vx2 tumor sections as a function of distance to the nearest vessel (Fig. 4D). A quantitative comparison of the mean fluorescent signal from doxorubicin within the Vx2 tumor but outside of CD31-stained regions (Fig. 4E) found a nearly 8.5-fold increase in doxorubicin fluorescence from the heated versus unheated tumor sections

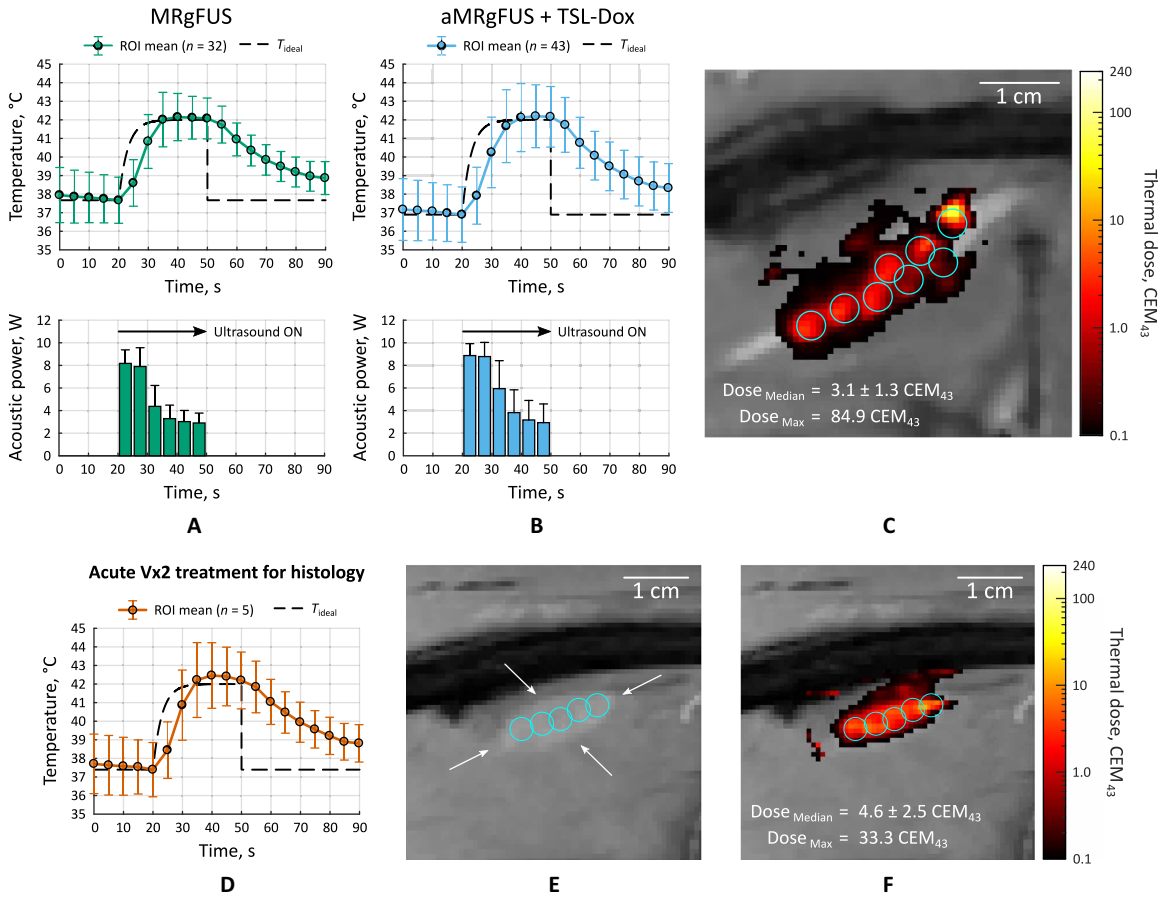

Fig. 3. MRgFUS temperature control and thermal dose deposition. Mean temperature ± SD across all Vx2 tumor ROIs used for real-time feedback control (top) and the applied acoustic power to achieve the temperature response (bottom) for the (**A**) MRgFUS alone group and the (**B**) MRgFUS+TSL-Dox group in the longitudinal tumor growth study. T_{ideal} was the temperature response that the controller attempted to achieve, and the time values on the horizontal axis are adjusted such that time 0 corresponds to 20 s before FUS was turned on. (**C**) Example image displaying the thermal dose in CEM_{43} overlaid upon the anatomical image of the Vx2 tumor that was heated with short-duration MRgFUS hyperthermia. All voxels with a thermal dose above 0.1 CEM_{43} are displayed in color, and the anatomy is shown in grayscale. (**D**) Mean temperatures ± SD of the heated ROIs in the heated Vx2 harvested for acute histology. (**E**) Vx2 tumor identification (white arrows) and ROI selection. (**F**) Thermal dose following the ultrashort MRgFUS thermal exposures in the heated Vx2 tumor.

[257 ± 47 AU (arbitrary units) versus 30 ± 12 AU, respectively; $^{***}P = 6 \times 10^{-6}$].

Antitumor effects of fractionated ultrashort MRgFUS hyperthermia and TSL-Dox

Follow-up contrast-enhanced T1-weighted images of rabbits bearing Vx2 thigh tumors showed a marked decrease in tumor size with TSL-Dox combined with short-duration MRgFUS hyperthermia (fig. S2). A timing diagram of the survival study is shown in (Fig. 5A). Of the six rabbits treated with MRgFUS+TSL-Dox, three survived to 120 days following treatment with complete destruction of the Vx2 tumor in four rabbits and only one reached the tumor size–related end point (Fig. 5B). All 11 rabbits receiving either MRgFUS or TSL-Dox alone reached the tumor size–related end point within 28 days following treatment. On the basis of a log-rank analysis of the survival data, there was a significant improvement in survival for the rabbits receiving MRgFUS+TSL-Dox compared to MRgFUS alone ($^{**}P = 0.002$) and compared to TSL-Dox alone ($^{**}P = 0.002$). The difference in survival benefit was not statistically significant between animals receiving MRgFUS or TSL-Dox alone ($P = 0.49$). The change in animal body weight as a function of time following treatment is shown in (Fig. 5C).

Rabbits receiving MRgFUS or TSL-Dox alone showed monotonic tumor progression, and all reached the tumor size–related end point within 28 days after treatment (Fig. 5, D to F). On the day of treatment, there was no significant difference among tumor volumes between each of the three treatment groups (Fig. 5G). At 1 week after treatment (Fig. 5H), the tumor volumes in the group that received MRgFUS alone were significantly greater than the group receiving MRgFUS+TSL-Dox (4.7 ± 2.7 cm^3 versus 0.9 ± 0.6 cm^3, respectively; $^{*}P = 0.01$). At 2 weeks after treatment (Fig. 5I), the tumor volumes in the groups receiving MRgFUS alone remained significantly greater than the group receiving MRgFUS+TSL-Dox (12.9 ± 5.0 cm^3 versus 0.8 ± 0.6 cm^3, respectively; $^{***}P = 0.0001$), but at this point, the group receiving TSL-Dox alone also had significantly larger tumor volumes than the group receiving MRgFUS+TSL-Dox (10.1 ± 3.5 cm^3 versus 0.8 ± 0.6 cm^3, respectively; $^{***}P = 0.0009$). No significant difference in tumor volumes was observed between the groups receiving MRgFUS or TSL-Dox alone.

Table 1. Physical characteristics and MRgFUS heating quality in Vx2 tumor–bearing rabbits. Rabbits were compared on several physical characteristics and several parameters associated with MRgFUS hyperthermia. The data are reported as the means ± SD with the range of values indicated in parentheses. Differences between groups were compared with an unpaired *t* test; all *P* values are two-sided, and a value of $^*P < 0.05$ was considered statistically significant.

Baseline characteristics	MRgFUS (*n* = 5)	MRgFUS+TSL-Dox (*n* = 6)	*P*
Body weight (kg)	3.4 ± 0.2 (3.1, 3.6)	3.3 ± 0.2 (2.9, 3.5)	0.46
Core temperature (°C)	35.0 ± 0.3 (34.6, 35.4)	34.9 ± 0.7 (33.9, 36.0)	0.62
Thigh temperature (°C)	34.7 ± 0.6 (33.9, 35.6)	34.2 ± 1.0 (32.8, 36.1)	0.43
MRgFUS hyperthermia results			
Acoustic energy deposited (kJ)	1.5 ± 0.2 (1.3, 1.7)	1.7 ± 0.2 (1.4, 1.9)	0.10
Treatment duration (min)	82.0 ± 16.9 (66, 110)	98.5 ± 24.6 (66, 134)	0.24
Heating duration above 40°C (min)	9.8 ± 4.8 (5.3, 14.9)	9.0 ± 10.5 (2.2, 29.8)	0.87
Temperature in the target region			
Mean (°C)	42.1 ± 0.3 (41.9, 42.4)	42.0 ± 0.4 (41.1, 42.5)	0.60
T_{10} (°C)	43.4 ± 0.4 (42.8, 43.7)	43.7 ± 0.6 (42.8, 44.5)	0.30
T_{90} (°C)	40.7 ± 0.4 (40.2, 41.1)	40.1 ± 0.7 (39.4, 41.2)	0.10
Thermal dose in the target region			
Median (CEM_{43})	2.8 ± 0.9 (1.8, 4.2)	3.2 ± 1.0 (1.7, 4.6)	0.54
T_{10} (CEM_{43})	7.9 ± 2.0 (5.7, 10.8)	14.0 ± 5.5 (6.1, 20.3)	0.04*
T_{90} (CEM_{43})	0.4 ± 0.2 (0.2, 0.6)	0.4 ± 0.5 (0.1, 1.4)	0.92

DISCUSSION

Thermosensitive liposomal drugs represent an important paradigm in oncology, where hyperthermia-mediated release coupled with thermal bioeffects enhance the effectiveness of chemotherapy. Their widespread clinical adoption hinges upon being able to control hyperthermia in a targeted manner, and temperature-based MRgFUS is a leading candidate to achieve this. This study represents the first demonstration of antitumor efficacy using novel fractionated ultrashort-duration hyperthermia exposures in combination with TSL-Dox. This approach was shown to potentiate the local release of doxorubicin from TSL-Dox and its subsequent uptake into Vx2 tumor tissue. The treatment resulted in a profound level of tumor growth inhibition and survival prolongation.

It is notable that fractionation has previously been investigated in hyperthermia, primarily in the context of potentiating radiotherapy. However, in these studies, heating was applied either sequentially or on separate days with individual exposures typically on the order of tens of minutes (*16*). The novel fractionated ultrashort paradigm examined here has several advantages over conventional long-duration hyperthermia. First, the strategy is compatible with breath holds, which mitigates tissue motion effects (*17*). This will improve targeting accuracy, as well as reduce the impact of motion on MRI-based temperature measurements used for feedback control. Second, shorter heating durations mitigate the convective cooling effects of blood perfusion (*18*). Hence, the fractionated ultrashort heating strategy will enable the treatment of a broader spectrum of tumors, such as those located in the liver, kidney, or the head and neck that are difficult to heat with conventional means.

It is important to consider the potential implications of ultrashort thermal dose fractionation on factors that will affect the net therapeutic effect of hyperthermia when combined with thermosensitive drugs. These include the degree of drug released, temperature-dependent biological effects (*19*), and temperature-dependent drug potentiation effects. An appropriate reference point for these considerations is the long-duration hyperthermia MRgFUS+TSL-Dox studies that have previously been conducted in the same rabbit thigh Vx2 tumor model (*14*, *15*, *20*). These studies demonstrated that controlled and targeted hyperthermia for tens of minutes produced local drug release, with the absolute concentration of doxorubicin delivered to the tumor increasing with heating duration over the time range of 10 to 40 min (*20*). A quantitative comparison of drug uptake in Vx2 tumor tissue between the present study and previous work was not conducted. However, in a direct comparison of the ultrashort heating paradigm presented here and continuous 20 min of heating using FUS, we showed that nearly half (49%) of the interstitial drug delivery was achieved in mouse tumors as measured with two-photon microscopy (*21*). With the ultrashort paradigm, total drug delivery can be increased by increasing the number of exposures at a particular location.

The present work has shown that substantial antitumor effects can also be achieved with the ultrashort heating method, and it is useful to compare these results with those previously obtained for continuous heating. In the study of Staruch *et al.* (*15*), 20 min of continuous heating to 42°C was combined with TSL-Dox in the same rabbit Vx2 tumor model and using the same doxorubicin dose of 1.67 mg/kg. It was observed that the MRgFUS+TSL-Dox group had significantly smaller tumor volumes than the TSL-Dox–only group at 2 weeks after treatment (1.1 ± 0.8 cm^3 versus 12.7 ± 4.7 cm^3, $P < 0.001$). These results are very similar to what we have presented here for the ultrashort heating paradigm where, at 2 weeks following treatment, the MRgFUS+TSL-Dox group was also significantly smaller than the group receiving TSL-Dox alone (0.8 ± 0.6 cm^3 versus 10.1 ± 3.5 cm^3, $P = 0.0009$). Furthermore, Staruch *et al.* observed that four of six rabbits that received MRgFUS+TSL-Dox survived 60 days following treatment, the latest time point in their tumor observation, versus zero of six for the TSL-dox alone group. In the present work with ultrashort exposures, the same result of four of six rabbits surviving to 60 days following treatment was obtained, with the additional observation that three of six rabbits survived to 120 days, which was the latest study time point.

In addition to drug delivery, the net therapeutic effect will also potentially be influenced by thermal bioeffects and thermal potentiation of drug effects, which have not been previously investigated for the exposure scheme used here. The similarity in treatment outcomes between the short- and long-duration approaches suggests that an investigation of bioeffects for the ultrashort exposures is warranted and would be valuable in refining this approach.

The precise control of short-duration heating exposures remains challenging because of the heterogeneity of tumor blood perfusion and flow in large vessels. It is expected that slight fluctuations about the target temperature will be observed in practice. The in vivo microscopy experiments presented here showed that temperature elevations from 41° to 45°C mediated the release of doxorubicin from ThermoDox and the delivery of the drug within a mouse dorsal skinfold window chamber tumor model. Others have shown that

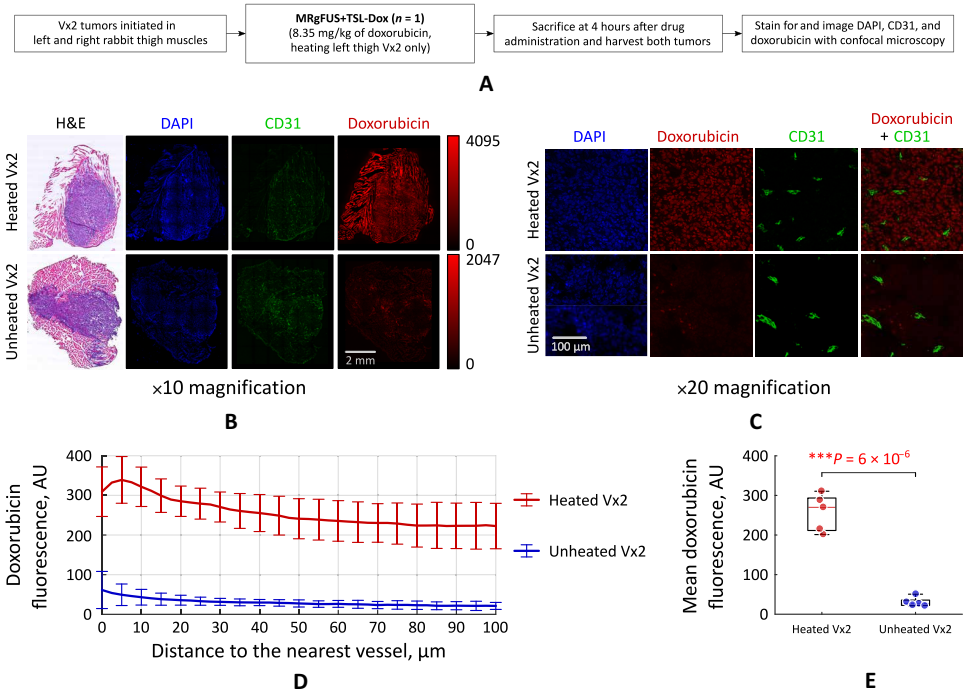

Fig. 4. Doxorubicin distribution in heated and unheated Vx2 tumors. (**A**) Experimental timeline for histological examination of heated and unheated Vx2 tumors. DAPI, 4′,6-diamidino-2-phenylindole. (**B**) Histological examination of bilateral Vx2 tumors, one heated and one unheated under ×10 magnification. Tumors were stained with hematoxylin and eosin (H&E) as well as DAPI for cell nucleus staining, CD31 expression on endothelial cells, and the fluorescence of doxorubicin, all of which were imaged with confocal microscopy. (**C**) Histological examination of bilateral Vx2 tumors under ×20 magnification. (**D**) Analysis of the doxorubicin fluorescence as a function of distance to the nearest vessel in heated and unheated tumors. The average data across $n = 5$ tumor sections spaced 250 µm apart were analyzed for both heated and unheated Vx2 tumors (AU, arbitrary units). (**E**) The mean fluorescent doxorubicin signal within the Vx2 tumor but outside CD31-stained endothelial cells was compared between all five tumor sections in both heated and unheated Vx2 tumors using an unpaired t test; $^{***}P < 0.001$.

temperature elevations greater than or equal to 43°C can result in blood flow cessation in preclinical tumor models (*22*), which may negatively affect drug delivery. This is consistent with the microscopy data that we have presented here, which showed evidence of microvessel hemorrhage during temperature elevations to 45°C that limited overall drug delivery. It is important to note that this is not observed to the same degree in human tumors (*23*) which, in general, have more mature neovasculature as well as co-opted healthy vessels (*24*). This contributes to a more robust tolerance to temperature elevation than experimental tumors in animals and may allow the tissue to spend more time above the temperature threshold required to release drug from TSL-Dox. The data that we have presented here also suggest that heating tumors to 41°C in ultrashort heat fractions will result in suboptimal drug release from TSL-Dox.

These results emphasize the notion that both underheating the tumor, which reduces intravascular TSL-Dox release, and overheating the tumor, which may damage the vasculature, limit intravascular drug delivery to the tumor site. In both cases, drug delivery from TSL-Dox is suboptimal, but it remains an open question whether the higher temperature elevations (e.g., 43° or 45°C) in the ultrashort heating context will confer additional therapeutically relevant antitumor bioeffects compared to the 42°C thermal exposures that we directly examined here; future work to this end is warranted.

One of the limitations of our rabbit tumor experiments was that the core temperature of rabbits was below physiological levels when TSL-Dox was administered. This likely increased the stability of the TSL-Dox, which begins to release drug at temperatures above 37°C, thus improving their circulation time. Future studies will take better care at maintaining the rabbit core body temperature at 36° to 37°C to more accurately inform the potential viability of the ultrashort heating strategy in human patients. A second limitation of our rabbit tumor experiments was the long treatment time associated with mechanically scanning a single-element transducer. Sophisticated phased-array transducers (*25*) could overcome the limitations of mechanically scanning a single-element transducer, providing the ability to uniformly heat larger areas of the tumor and reduce treatment times in the clinical context for human patients.

These results have considerable implications for the widespread clinical adoption of thermosensitive drugs in oncology. The flexibility and noninvasive nature of MRgFUS makes it a very attractive therapeutic modality whereby treatment plans are easily adjusted, and large volumes can be treated without any surgical procedures or ionizing radiation. MRgFUS can achieve mild temperature elevations within the hyperthermia regime (*26*) as well as high-temperature ablations, both of which can be combined with thermosensitive drugs (*27*). Several groups have developed thermosensitive drug delivery systems that incorporate other forms of commonly used chemotherapeutic agents, such as cisplatin (*28*), that can be delivered with MRgFUS hyperthermia, and some have begun to evaluate multiple thermosensitive drug cocktails to maximize tumor-specific cytotoxicity (*29*). Therefore, by overcoming the limitations on clinical MRgFUS hyperthermia, this noninvasive treatment strategy can be used on a broader spectrum of tumor indications to both improve patient outcomes and reduce treatment-associated side effects.

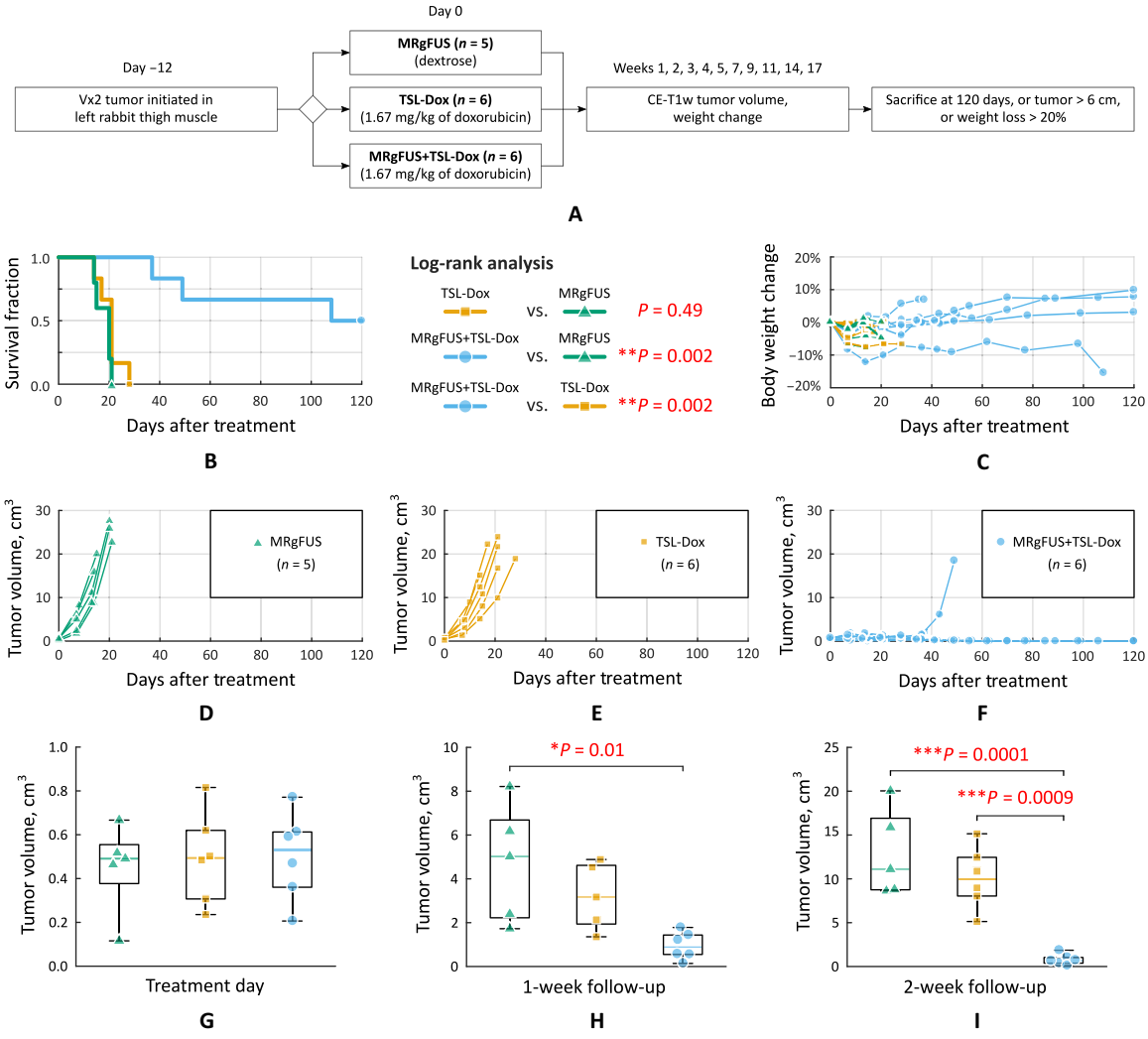

Fig. 5. Vx2 tumor growth following MRgFUS and TSL-Dox. (**A**) Survival study design where rabbits were randomly assigned into one of three treatment groups. Following treatment tumor volumes were measured with contrast-enhanced (CE) T1w MR images. (**B**) Kaplan-Meier survival analysis where groups were compared with a log-rank test and a Bonferroni correction for multiple comparisons; $^{**}P < 0.01$. (**C**) Percent change in animal body weight after treatment. Tumor growth curves for the animals receiving MRgFUS alone (**D**) TSL-Dox alone (**E**) and the combination of MRgFUS+TSL-Dox (**F**). Tumor volume comparison on the day of treatment (**G**) at 1 week after treatment (**H**) and at 2 weeks following treatment (**I**). Groups were compared with a one-way ANOVA and a Bonferroni correction for multiple comparisons; $^{*}P < 0.05$, $^{**}P < 0.01$, and $^{***}P < 0.001$.

MATERIALS AND METHODS

Dorsal skinfold window chamber tumor model and FUS hyperthermia

To investigate the microscale drug distribution from ultrashort (10×, ~30 s) thermal exposures (41°, 42°, 43°, or 45°C) and a commercial formulation of TSL-Dox (ThermoDox, Celsion Corporation, Lawrenceville, NJ), human FaDu tumor cells expressing GFP (FaDu-GFP, AntiCancer Inc., San Diego, CA) were implanted into the skinfold of male BALB/c nude mice ($n = 22$) and allowed to grow for 9 to 12 days whereupon experiments commenced. A detailed description of the tumor model and surgical preparation (*30*) can be found in the Supplementary Materials. All animal studies were approved by the Animal Care Committee at the Sunnybrook Research Institute in Toronto, Canada.

Two-photon imaging procedures

To visualize the FaDu-GFP tumor vasculature, FITC-dextran (2 MDa; Invitrogen, Burlington, Canada) was injected as an intravascular bolus through the tail vein at a dose of 33 mg/kg dissolved in phosphate-buffered saline. Two-photon imaging was performed using a 25×/1.05 numerical aperture (NA) water immersion objective lens (XL25XWMP; Olympus, Tokyo, Japan) with a 509 × 509 μm field of view (512 × 512 pixels). Laser scanning was performed with a two-photon microscope (FVMPE-RS, Olympus, Tokyo, Japan) and an InSight DeepSee mode-locked titanium-sapphire tunable laser (509 μm by 509 μm; Newport Corp., Irvine, CA). The FaDu-GFP cells and collagen were excited at 900 nm, and the FITC-labeled vasculature and doxorubicin were excited at 810 nm. The fluorescence emissions were collected by photomultiplier tubes following band-pass filtering of 440/40 nm for collagen, 515/50 nm for FITC and FaDu-GFP, and 600/50 nm for doxorubicin.

Once a tumor vessel bed was selected, a baseline XYZ volume stack was acquired at 810 nm to create a three-dimensional (3D) vascular map of the tumor vessels. Lateral images 512 × 512 pixels were acquired below the coverslip up to 150 μm in depth in 2-μm

increments. These volumes were acquired every 6 min. Interleaved between volume stacks, single-plane XYT acquisitions were performed with increased temporal resolution (915 frames, 65.8 ms per frame) for a total duration of 60 s to visualize the intravascular release of doxorubicin from TSL-Dox in real time during the ultrashort thermal exposures that were performed during these XYT acquisitions. The doxorubicin fluorescence expressed in normalized units (% I_0) at each time point was calculated in the following way

$$\% I_0 = \frac{I_t - I_0}{I_0} \times 100\% \quad (1)$$

where the fluorescent signal in the doxorubicin channel at time t (denoted as I_t) was corrected for FITC bleed-through and normalized with respect to the baseline fluorescent signal (I_0) in each compartment for analysis (intravascular and extravascular).

To quantify the drug release in real time during each XYT scan, 2D vascular masks were created and the baseline fluorescent signal (I_0) was calculated from the average of the first ~5 s of image acquisition (75 frames) in each acquisition before the start of FUS heating. The mean intravascular signal during the remainder of the acquisition was calculated and normalized to the baseline signal level at each time point. Drug penetration depth was measured for the XYZ data by performing a Euclidean distance transform of the segmented 3D vascular mask to create a distance map from each extravascular pixel to the nearest vascular structure. The baseline fluorescent signal in this case was measured before the first XYZ acquisition. The mean fluorescent signal for pixels at each distance from the nearest vessel was reported up to 35 μm.

FUS hyperthermia during two-photon microscopy

To allow simultaneous FUS hyperthermia and two-photon microscopy, an ultrasonic ring transducer was used and driven at a frequency of 1.2 MHz (*31*). The applied power to the ring transducer was modulated on the basis of temperature feedback from two implanted thermocouples at a rate of 1 Hz. The thermocouples were made by soldering the tips of a copper and a constantan wire (50-μm diameter) in a twister pair. The intensity distribution produced by the ring transducer is shown in fig. S3. The thermocouples were not placed directly in the center of the window chamber, where the peak intensity is produced, to prevent the generation of a viscous heating artifact, which would make the temperature measurements inaccurate (*32*). Tumor temperatures were elevated from baseline to 41°, 42°, 43°, and 45°C in 15 s and maintained for an additional 15 s during real-time two-photon microscopy. Following each hyperthermia exposure, the tissue could return to baseline over 5 min before being heated again for a total of 10 times. A description of the PID control algorithm used for these experiments has been described previously (*21*).

Rabbit Vx2 tumor model

MRgFUS experiments were performed in male New Zealand white rabbits (n = 18) that were housed with food and water given ad libitum throughout the study period. Vx2 tumor cells were prepared from frozen tumor pieces stored in Hanks' balanced salt solution in 2-ml cryogenic tubes at −80°C. On the day of tumor initiation, tumor pieces were thawed in a 37°C water bath, and an injection of 0.8 million Vx2 cells in a total volume of 100 μl was prepared. Vx2 tumors were subsequently initiated in the left thigh muscle of rabbits and grew for 12 to 13 days whereupon experiments commenced. More details of the tumor cell preparation and implantation can be found in the Supplementary Materials.

Fractionated ultrashort MRgFUS thermal exposures in Vx2 tumors

Ultrashort MRgFUS thermal exposures were achieved with a single-element spherically curved air-backed transducer (diameter, 100 mm; radius of curvature, 80 mm), driven at 1.515 MHz with a mode 2 acoustic lens (*33*) (intensity distribution shown in fig. S4, heating distribution in fig. S5) within an MRI-compatible three-axis positioning system (similar in function to LP-100, FUS Instruments Inc., Toronto, Canada). On the day of treatment, animals were anesthetized with a mixture of ketamine (50 mg/kg; Vétoquinol, Magny-Vernois, France) and xylazine (5 mg/kg; Bayer Inc., Toronto, Canada) administered as an intramuscular bolus away from the heated region. Animals were then intubated, and anesthesia was maintained with 2 to 3% isoflurane for the duration of the treatment. The marginal ear vein was catheterized to allow the injection of TSL-Dox and gadolinium-based MRI contrast agent. A pulse oximeter (Model 8600 V; Nonin Medical Inc., Plymouth, MN) was attached to the animal's paw following removal of excess fur with clippers to monitor heart rate and oxygen saturation. To facilitate acoustic coupling, the hair from the thighs was removed with electric clippers and depilatory lotion (Nair; Church and Dwight Co., Princeton, NJ). To minimize the risk of hot spots created at skin-air interfaces in the far field (*34*), a degassed water bag was placed between the rabbit's legs and coupled to the skin with ultrasound gel following hair removal.

Body (rectal) and thigh muscle temperatures away from the focal region were recorded using fiber-optic probes (Reflex Signal Conditioner; Neoptix, Québec City, Canada) and averaged to provide a baseline temperature for MR thermometry. A heated water blanket was used to maintain the core body temperature of the animal, and a second pump sent heated water through a heating coil below the targeted thigh to help maintain temperature uniformity. The heated thigh was coupled to the degassed water bath of the positioning system with ultrasound gel atop an acoustically transparent polyimide membrane.

MR thermometry was used to provide real-time temperature feedback during the ultrashort thermal exposures. The FUS transducer and positioning system was placed in a clinical MRI suite (MR750 Discovery 3.0T; GE Healthcare, Chicago, IL). A single-loop receive-only coil with a square opening of 11 cm was placed underneath the animal to improve image quality. Vx2 tumors were identified in rabbit thigh muscle with contrast-enhanced [gadobutrol (0.05 mmol/kg), Gadovist; Bayer Inc., Mississauga, Canada) T1-weighted MR images. Because of the potential for gadolinium to cause errors in MR thermometry measurements, we allowed 51.1 ± 15.0 min (ranging from 34 to 90 min) to elapse before MR thermometry began such that much of the gadolinium could be cleared from circulation. Following tumor delineation, several 4.5-mm-diameter ROIs were placed over target locations to cover the tumor. This resulted in five to eight discrete ROIs in to cover all the tumors that were heated in this study. Each ROI was discretely heated a total of 10 times, and during each sonication, ultrasound was applied for 30 s and the tissue could cool for an additional 30 s before the transducer was moved to target the next ROI. The sequence in which the ROIs were heated was chosen to prevent heating adjacent ROIs wherever possible to prevent overheating individual portions of the tumor.

During heating, the temperature across the focus of the transducer within the tumor was continuously monitored using temperature maps calculated on the basis of the proton resonant frequency (PRF) shift MR thermometry method (*35*). A fast-spoiled gradient-echo sequence (3-mm slice thickness, 5-s temporal resolution) was used for thermometry with the temperature dependence of the PRF shift in rabbit skeletal muscle ($\alpha = -0.00909$ parts per million/°C) (*36*). Both the real and imaginary parts of the MR image data were used to process the temperature maps (*37*).

To achieve and maintain accurate temperature maps for feedback control of the MRgFUS sonication, a 2D first-order iterative drift correction was applied to compensate for magnetic field drift and field perturbations caused by transducer movement throughout the imaging duration. The compensation technique was based on the hybrid multibaseline and referenceless method of MR thermometry described by Grissom *et al.* (*38*, *39*) using 30 baseline library images, 25 iterations, a first-order 2D polynomial, and a regularization parameter of 10^{-2}. During the baseline library acquisition, the transducer was mechanically scanned across each of the treatment locations and held at each position for a minimum of three images.

For short-duration (~30 s) mild hyperthermia (42°C), a combined "bang-bang" and conventional proportional, integral, and derivative (PID) control strategy was used (*40*). The acoustic power level was updated with each thermometry image (subscript *i*) based on the following equation

$$P_{\text{out}} = \begin{cases} P_{\text{max\_BANG}} & T < 40°\text{C} \\ P_{i-1} + \Delta P \le P_{\text{max\_PID}} & 40°\text{C} \le T \le 43°\text{C} \\ 0 & T > 43°\text{C} \end{cases} \quad (2)$$

where P_{out} is the output acoustic power level and $P_{\text{max\_BANG}}$ is both the starting power level and the output power whenever the mean temperature within the ROI was found to be below 40°C. $P_{\text{max\_BANG}}$ ranged from 7.5 to 10.0 W of acoustic power. Once the mean temperature went above 40°C, the acoustic power was immediately dropped to $P_{\text{max\_PID}}$ and was adjusted using a PID control algorithm if the mean temperature remained below 43°C. $P_{\text{max\_PID}}$ ranged from 3.5 to 5.0 W. If at any point the mean temperature went above 43°C, then the power would be turned off. The PID error term, ΔP, was determined by the following equation

$$\Delta P = K_{\text{P}} e_i + K_{\text{I}} \sum_{j=0}^{j=i} e_j + K_{\text{D}}(e_{i-1} - e_i) \quad (3)$$

where e_i is the difference between the measured temperature and the ideal temperature response. K_{P} is the proportional gain, K_{I} is the integral gain and K_{D} is the derivative gain, which were empirically determined to be 800, 1, and 75 mW/°C, respectively. To reduce the initial accumulation of error during heating, the ideal temperature response at time *t* was prescribed as an exponential ramp instead of a step function (*41*)

$$T_{\text{ideal}}(t) = (T_{\text{goal}} - T_{\text{baseline}}) \cdot e^{-5t/\tau} + T_{\text{baseline}} \quad (4)$$

where T_{goal} was 42°C and the time constant τ was chosen to be 15 s. Thermal dose in the target region was calculated in CEM_{43} using the Sapareto-Dewey time-temperature equation (*42*).

At the maximum power level used in this study, the in situ spatial-peak temporal average intensity (I_{SPTA}) was 45 W/cm^2 and the in situ peak pressure amplitude was 1.2 MPa. These values account for propagation through 2 mm of skin (22 Np/m) and 10 mm of muscle tissue (6.3 Np/m) whose attenuation values were based on the frequency-dependent tissue parameters for a frequency of 1.515 MHz (*43*). The in situ peak pressure amplitude falls well below the inertial cavitation threshold in skeletal muscle at 1.515 MHz, which is approximately 8.6 MPa (*44*).

Imaging doxorubicin delivery to heated and unheated Vx2 tumors

Bilateral Vx2 thigh tumors were initiated in $n = 1$ rabbit to examine the doxorubicin distribution following ultrashort MRgFUS thermal exposures with TSL-Dox as described above at a 5× dose (8.35 mg/kg of doxorubicin) compared to the dose level in the survival study. Following the heating of the left thigh tumor, the rabbit was sacrificed at 4 hours after drug administration, and both the left and right thigh tumors were harvested. The tumors were immediately placed in optimum cutting temperature compound (Tissue-Tek, Torrance, CA) and stored at −80°C before tissue sectioning and immunohistochemical staining. A total of five cryostat sections 10 μm thick and 250 μm apart were cut from each tumor, mounted on glass slides, and allowed to air dry. Fluorescent imaging was performed using an inverted confocal laser scanning microscope (A1+; Nikon, Tokyo, Japan).

Doxorubicin autofluorescence was detected with 487.9-nm excitation and 595/50-nm emission filters. Entire tissue sections were imaged and tiled with a motorized stage using a 10×/0.45 NA objective lens for quantitative analysis, and a 20×/0.75 NA objective was used to image ROIs at increased resolution for a qualitative comparison between heated and unheated tumors.

Blood vessels in tissue sections were recognized by the expression of CD31 on endothelial cells. Following doxorubicin imaging, tissue sections were stained with a mouse anti-CD31 (1:500, ab212712; Abcam Inc., Cambridge, MA) primary antibody for 60 min. Next, tissue sections were washed in phosphate-buffered saline and stained with a donkey anti-mouse immunoglobulin G Alexa Fluor 647 secondary antibody (1:1000, ab150107; Abcam Inc., Cambridge, MA) for 30 min before the addition of an aqueous mounting media (Fluoroshield with DAPI, Sigma-Aldrich Corporation, St. Louis, MO) and allowed to air-dry before fluorescent imaging. Tissue sections were then reimaged in an identical way as was used to capture doxorubicin fluorescence. Alexa Fluor 647 fluorescence representing endothelial cells was captured using 639.1-nm excitation and 700/75-nm emission filters. DAPI fluorescence representing tumor cell nuclei was captured using 403.1-nm excitation and 450/50-nm emission filters. Tissue sections were subsequently stained with hematoxylin to delineate nuclear morphology.

Images displaying anti-CD31 staining were converted to a binary image, and objects <62 μm^2 were removed on the basis of a conservative estimate of minimal capillary diameter (*45*). The resultant image was overlaid with the corresponding field of view displaying doxorubicin fluorescence. ROIs within the Vx2 tumor were selected from each tissue section and were, on average, ~2.5 mm^2. The regions selected for analysis did not include regions of necrosis or staining artifacts. A minimum signal level just below the threshold for the detection of doxorubicin was set for each tissue section (*46*), and this level was based on an average background reading from regions without nuclear fluorescence/staining. The mean fluorescent intensity for all pixels above the threshold was calculated as a function of the distance to the nearest CD31-stained pixel and compared

between heated and unheated tumor sections. The mean fluorescent intensity of all pixels above the threshold was also calculated as a measure of the total drug concentration within each tumor section for comparison. A photograph of the freshly excised tumors is shown in fig. S6, illustrating the red color visible within the heated tumor (red is the color of doxorubicin).

Survival study design

Rabbits with Vx2 tumors in their left thigh muscle were randomly assigned into one of three treatment groups: MRgFUS alone ($n = 5$), TSL-Dox alone ($n = 6$), or MRgFUS+TSL-Dox ($n = 6$). In groups receiving TSL-Dox, rabbits were administered a dose of 1.67 mg doxorubicin/kg body weight diluted in 5% dextrose as a slow bolus, over 3 min. Characterization of the in-house TSL-Dox, based on (*47*), that was used in the MRgFUS experiments can be found in fig. S7 and table S2.

Following treatment, tumor volumes were measured with contrast-enhanced MRI on a weekly basis for the first 2 months and biweekly after that until 120 days after treatment. The MR scan parameters can be found in table S3. Tumor volumes were calculated from manually contouring the enhanced tumor region on sagittal slices, multiplying by the slice thickness and summing through all images where the tumor was present. Animals were sacrificed if the Vx2 tumor exceeded 6 cm in its longest dimension or if animal body weight fell below 80% of its value on the day of tumor initiation.

Statistical analysis

The mean extravascular signal in mouse tumors at 60 min following the infusion of TSL-Dox and Vx2 tumor volumes were compared using a one-way analysis of variance (ANOVA) with Bonferroni post hoc tests for multiple comparisons in MATLAB. Differences in tumor doxorubicin fluorescence within heated and unheated tumors was compared with an unpaired t test in MATLAB. Differences in rabbit survival were compared with a log-rank test and a Bonferroni correction for multiple comparisons using GraphPad Prism 5.0 software. All P values were two-sided, and a value of $P < 0.05$ was considered significant in all cases.

SUPPLEMENTARY MATERIALS

Supplementary material for this article is available at http://advances.sciencemag.org/cgi/content/full/6/36/eaba5684/DC1

View/request a protocol for this paper from *Bio-protocol*.

REFERENCES AND NOTES

1. M. B. Yatvin, J. N. Weinstein, W. H. Dennis, R. Blumenthal, Design of liposomes for enhanced local release of drugs by hyperthermia. *Science* **202**, 1290–1293 (1978).
2. S. Stapleton, M. Dunne, M. Milosevic, C. W. Tran, M. J. Gold, A. Vedadi, T. D. Mckee, P. S. Ohashi, C. Allen, D. A. Jaffray, Radiation and heat improve the delivery and efficacy of nanotherapeutics by modulating intratumoral fluid dynamics. *ACS Nano* **12**, 7583–7600 (2018).
3. G. Kong, R. D. Braun, M. W. Dewhirst, Hyperthermia enables tumor-specific nanoparticle delivery: Effect of particle size. *Cancer Res.* **60**, 4440–4445 (2000).
4. A. Sen, M. L. Capitano, J. A. Spernyak, J. T. Schueckler, S. Thomas, A. K. Singh, S. S. Evans, B. L. Hylander, E. A. Repasky, Mild elevation of body temperature reduces tumor interstitial fluid pressure and hypoxia and enhances efficacy of radiotherapy in murine tumor models. *Cancer Res.* **71**, 3872–3880 (2011).
5. J. J. Skitzki, E. A. Repasky, S. S. Evans, Hyperthermia as an immunotherapy strategy for cancer. *Curr. Opin. Investig. Drugs* **10**, 550–558 (2009).
6. G. M. Hahn, J. Braun, I. Har-Kedar, Thermochemotherapy: Synergism between hyperthermia (42-43 degrees) and adriamycin (of bleomycin) in mammalian cell inactivation. *Proc. Natl. Acad. Sci. U.S.A.* **72**, 937–940 (1975).
7. R. D. Issels, Hyperthermia adds to chemotherapy. *Eur. J. Cancer* **44**, 2546–2554 (2008).
8. Y. N. Dou, J. Zheng, W. D. Foltz, R. Weersink, N. Chaudary, D. A. Jaffray, C. Allen, Heat-activated thermosensitive liposomal cisplatin (HTLC) results in effective growth delay of cervical carcinoma in mice. *J. Control. Release* **178**, 69–78 (2014).
9. W. Y. Tak, S.-M. Lin, Y. Wang, J. Zheng, A. Vecchione, S. Y. Park, M. H. Chen, S. Wong, R. Xu, C.-Y. Peng, Y.-Y. Chiou, G.-T. Huang, J. Cai, B. J. J. Abdullah, J. S. Lee, J. Y. Lee, J.-Y. Choi, J. Gopez-Cervantes, M. Sherman, R. S. Finn, M. Omata, M. O'Neal, L. Makris, N. Borys, R. Poon, R. Lencioni, Phase III HEAT study adding lyso-thermosensitive liposomal doxorubicin to radiofrequency ablation in patients with unresectable hepatocellular carcinoma lesions. *Clin. Cancer Res.* **24**, 73–83 (2018).
10. C. J. Diederich, K. Hynynen, Ultrasound technology for hyperthermia. *Ultrasound Med. Biol.* **25**, 871–887 (1999).
11. M. D. Gray, P. C. Lyon, C. Mannaris, L. K. Folkes, M. Stratford, L. Campo, D. Y. F. Chung, S. Scott, M. Anderson, R. Goldin, R. Carlisle, F. Wu, M. R. Middleton, F. V. Gleeson, C. C. Coussios, Focused ultrasound hyperthermia for targeted drug release from thermosensitive liposomes: Results from a phase I trial. *Radiology* **291**, 232–238 (2019).
12. K. Hynynen, Hyperthermia-induced drug delivery in humans. *Nat. Biomed. Eng.* **2**, 637–639 (2018).
13. K. Hynynen, A. Darkazanli, E. Unger, J. F. Schenck, MRI-guided noninvasive ultrasound surgery. *Med. Phys.* **20**, 107–115 (1993).
14. A. Ranjan, G. C. Jacobs, D. L. Woods, A. H. Negussie, A. Partanen, P. S. Yarmolenko, C. E. Gacchina, K. V. Sharma, V. Frenkel, B. J. Wood, M. R. Dreher, Image-guided drug delivery with magnetic resonance guided high intensity focused ultrasound and temperature sensitive liposomes in a rabbit Vx2 tumor model. *J. Control. Release* **158**, 487–494 (2012).
15. R. M. Staruch, K. Hynynen, R. Chopra, Hyperthermia-mediated doxorubicin release from thermosensitive liposomes using MR-HIFU: Therapeutic effect in rabbit Vx2 tumours. *Int. J. Hyperthermia* **31**, 118–133 (2015).
16. M. K. Lam, C. Oerlemans, M. Froeling, R. Deckers, A. D. Barten-Van Rijbroek, M. A. Viergever, C. T. W. Moonen, C. Bos, L. W. Bartels, DCE-MRI and IVIM-MRI of rabbit Vx2 tumors treated with MR-HIFU-induced mild hyperthermia. *J. Ther. Ultrasound.* **4**, 9 (2016).
17. C. Bing, B. Cheng, R. M. Staruch, J. Nofiele, M. Wodzak Staruch, D. Szczepanski, A. Farrow-Gillespie, A. Yang, T. W. Laetsch, R. Chopra, Breath-hold MR-HIFU hyperthermia: Phantom and in vivo feasibility. *Int. J. Hyperthermia* **36**, 1084–1097 (2019).
18. B. E. Billard, K. Hynynen, R. B. Roemer, Effects of physical parameters on high temperature ultrasound hyperthermia. *Ultrasound Med. Biol.* **16**, 409–420 (1990).
19. P. Wust, B. Hildebrandt, G. Sreenivasa, B. Rau, J. Gellermann, H. Riess, R. Felix, P. Schlag, Hyperthermia in combined treatment of cancer. *Lancet Oncol.* **3**, 487–497 (2002).
20. C. Bing, P. Patel, R. M. Staruch, S. Shaikh, J. Nofiele, M. Wodzak Staruch, D. Szczepanski, N. S. Williams, T. Laetsch, R. Chopra, Longer heating duration increases localized doxorubicin deposition and therapeutic index in Vx2 tumors using MR-HIFU mild hyperthermia and thermosensitive liposomal doxorubicin. *Int. J. Hyperthermia* **36**, 196–203 (2019).
21. M. A. Santos, D. E. Goertz, K. Hynynen, Focused ultrasound hyperthermia mediated drug delivery using thermosensitive liposomes and visualized with in vivo two-photon microscopy. *Theranostics.* **7**, 2718–2731 (2017).
22. T. E. Dudar, R. K. Jain, Differential response of normal and tumor microcirculation to hyperthermia. *Cancer Res.* **44**, 605–612 (1984).
23. F. M. Waterman, R. E. Nerlinger, D. J. Moylan III, D. B. Leeper, Response of human tumor blood flow to local hyperthermia. *Int. J. Radiat. Oncol. Biol. Phys.* **13**, 75–82 (1987).
24. E. A. Kuczynski, P. B. Vermeulen, F. Pezzella, R. S. Kerbel, A. R. Reynolds, Vessel co-option in cancer. *Nat. Rev. Clin. Oncol.* **16**, 469–493 (2019).
25. P. Aslani, L. Drost, Y. Huang, B. B. C. Lucht, E. Wong, G. Czarnota, C. Yee, B. A. Wan, V. Ganesh, S. T. Gunaseelan, E. David, E. Chow, K. Hynynen, Thermal therapy with a fully electronically steerable HIFU phased array using ultrasound guidance and local harmonic motion monitoring. *I.E.E.E. Trans. Biomed. Eng.* **67**, 1854–1862 (2019).
26. M. de Smet, N. M. Hijnen, S. Langereis, A. Elevelt, E. Heijman, L. Dubois, P. Lambin, H. Grüll, Magnetic resonance guided high-intensity focused ultrasound mediated hyperthermia improves the intratumoral distribution of temperature-sensitive liposomal doxorubicin. *Invest. Radiol.* **48**, 395–405 (2013).
27. N. Hijnen, E. Kneepkens, M. de Smet, S. Langereis, E. Heijman, H. Grüll, Thermal combination therapies for local drug delivery by magnetic resonance-guided high-intensity focused ultrasound. *Proc. Natl. Acad. Sci. U.S.A.* **114**, E4802–E4811 (2017).
28. M. Dunne, Y. N. Dou, D. M. Drake, T. Spence, S. M. L. Gontijo, P. G. Wells, C. Allen, Hyperthermia-mediated drug delivery induces biological effects at the tumor and molecular levels that improve cisplatin efficacy in triple negative breast cancer. *J. Control. Release* **282**, 35–45 (2018).
29. M. Dunne, B. Epp-Ducharme, A. M. Sofias, M. Regenold, D. N. Dubins, C. Allen, Heat-activated drug delivery increases tumor accumulation of synergistic chemotherapies. *J. Control. Release* **308**, 197–208 (2019).
30. G. M. Palmer, A. N. Fontanella, S. Shan, G. Hanna, G. Zhang, C. L. Fraser, M. W. Dewhirst, In vivo optical molecular imaging and analysis in mice using dorsal window chamber

models applied to hypoxia, vasculature and fluorescent reporters. *Nat. Protoc.* **6**, 1355–1366 (2011).
31. T. Nhan, A. Burgess, K. Hynynen, Transducer design and characterization for dorsal-based ultrasound exposure and two-photon imaging of in vivo blood-brain barrier disruption in a rat model. *IEEE Trans. Ultrason. Ferroelectr. Freq. Control* **60**, 1376–1385 (2013).
32. K. Hynynen, D. K. Edwards, Temperature measurements during ultrasound hyperthermia. *Med. Phys.* **16**, 618–626 (1989).
33. T. Fjield, V. Sorrentino, H. Cline, K. Hynynen, Design and experimental verification of thin acoustic lenses for the coagulation of large tissue volumes. *Phys. Med. Biol.* **42**, 2341–2354 (1997).
34. K. Hynynen, Hot spots created at skin-air interfaces during ultrasound hyperthermia. *Int. J. Hyperthermia* **6**, 1005–1012 (1990).
35. Y. Ishihara, A. Calderon, H. Watanabe, K. Okamoto, Y. Suzuki, K. Kuroda, Y. Suzuki, A precise and fast temperature mapping using water proton chemical shift. *Magn. Reson. Med.* **34**, 814–823 (1995).
36. A. H. Chung, F. A. Jolesz, K. Hynynen, Thermal dosimetry of a focused ultrasound beam in vivo by magnetic resonance imaging. *Med. Phys.* **26**, 2017–2026 (1999).
37. A. H. Chung, K. Hynynen, V. Colucci, K. Oshio, H. E. Cline, F. A. Jolesz, Optimization of spoiled gradient-echo phase imaging for in vivo localization of a focused ultrasound beam. *Magn. Reson. Med.* **36**, 745–752 (1996).
38. W. A. Grissom, M. Lustig, A. B. Holbrook, V. Rieke, J. M. Pauly, K. Butts-Pauly, Reweighted ℓ_1 referenceless PRF shift thermometry. *Magn. Reson. Med.* **64**, 1068–1077 (2010).
39. W. A. Grissom, V. Rieke, A. B. Holbrook, Y. Medan, M. Lustig, J. Santos, M. V. McConnell, K. B. Pauly, Hybrid referenceless and multibaseline subtraction MR thermometry for monitoring thermal therapies in moving organs. *Med. Phys.* **37**, 5014–5026 (2010).
40. W.-L. Lin, R. B. Roemer, K. Hynynen, Theoretical and experimental evaluation of a temperature controller for scanned focused ultrasound hyperthermia. *Med. Phys.* **17**, 615–625 (1990).
41. E. Hutchinson, M. Dahleh, K. Hynynen, The feasibility of MRI feedback control for intracavitary phased array hyperthermia treatments. *Int. J. Hyperthermia* **14**, 39–56 (1998).
42. S. A. Sapareto, W. C. Dewey, Thermal dose determination in cancer therapy. *Int. J. Radiat. Oncol. Biol. Phys.* **10**, 787–800 (1984).
43. F. A. Duck, *Physical Properties of Tissues: A Comprehensive Reference Book* (Academic Press, 2012).
44. K. Hynynen, The threshold for thermally significant cavitation in dog's thigh muscle in vivo. *Ultrasound Med. Biol.* **17**, 157–169 (1991).
45. J. R. Less, T. C. Skalak, E. M. Sevick, R. K. Jain, Microvascular architecture in a mammary carcinoma: Branching patterns and vessel dimensions. *Cancer Res.* **51**, 265–273 (1991).
46. A. J. Primeau, A. Rendon, D. Hedley, L. Lilge, I. F. Tannock, The distribution of the anticancer drug Doxorubicin in relation to blood vessels in solid tumors. *Clin. Cancer Res.* **11**, 8782–8788 (2005).
47. B. L. Viglianti, M. W. Dewhirst, R. J. Boruta, J.-Y. Park, C. Landon, A. N. Fontanella, J. Guo, A. Manzoor, C. L. Hofmann, G. M. Palmer, Systemic anti-tumour effects of local thermally sensitive liposome therapy. *Int. J. Hyperthermia* **30**, 385–392 (2014).

Acknowledgments: We would like to thank V. Chan and S. Rideout-Gros for help with tumor initiation and animal monitoring during experiments; L. Wang, J. Steigenberger, and E. Siniscalchi for help with the manufacturing and characterization of thermosensitive liposomal doxorubicin; J. Sun for performing the Vx2 tumor sectioning and immunohistochemical staining; G. Awong for instruction on how to operate the confocal laser scanning microscope; D. McMahon for many helpful discussions regarding antibody selection, confocal microscopy techniques and editing the manuscript; and C. Poon for editing the manuscript. ThermoDox was provided by Celsion Corporation. **Funding:** This work was supported by a Canadian Cancer Society Impact Grant, the Ontario Institute for Cancer Research, and the Canada Research Chairs Program. **Author contributions:** M.A.S., S.-K.W., D.E.G., and K.H. designed the experiments. M.R. and C.A. designed, manufactured, and characterized the thermosensitive liposomal doxorubicin. M.A.S. performed the microscopy experiments. M.A.S. and S.-K.W. performed the MRgFUS experiments. M.A.S. analyzed the data. M.A.S., S.-K.W., C.A., D.E.G., and K.H. interpreted the data. M.A.S., M.R., C.A., D.E.G., and K.H. wrote the manuscript. All authors approved of the manuscript in its final form. **Competing interests:** M.A.S. has done paid work for FUS Instruments Inc. (a manufacturer of preclinical ultrasound research devices). C.A. acknowledges a Research Chair in Pharmaceutics and Drug Delivery from GlaxoSmithKline Inc. (a company that develops and manufactures pharmaceutical medicines, vaccines, and consumer healthcare products). K.H. owns stocks in, is a board member of, and receives research funding from FUS Instruments Inc. (a manufacturer of preclinical ultrasound research devices) and Harmonic Medical Inc. (which is developing thermal ablation devices for clinical use). The authors declare that they have no additional competing interests. **Data and materials availability:** All relevant data that support this study as well as the MATLAB code used to analyze it are available from the corresponding author upon reasonable request. All data needed to evaluate the conclusions in the paper are present in the paper and/or the Supplementary Materials. Additional data related to this paper may be requested from the authors.

Submitted 8 January 2020
Accepted 20 July 2020
Published 2 September 2020
10.1126/sciadv.aba5684

Citation: M. A. Santos, S.-K. Wu, M. Regenold, C. Allen, D. E. Goertz, K. Hynynen, Novel fractionated ultrashort thermal exposures with MRI-guided focused ultrasound for treating tumors with thermosensitive drugs. *Sci. Adv.* **6**, eaba5684 (2020).